

## DEVELOPMENT AND OPERATION OF A PROTOTYPE SUPERCONDUCTING LINAC FOR HEAVY-ION ACCELERATION\*

J. Aron, R. Benaroya, L. M. Bollinger, K. E. Gray, A. H. Jaffey, F. J. Lynch, K. W. Johnson, T. K. Khoo, J. J. Livingood, J. M. Nixon, G. W. Parker, W. J. Ramler, and W. A. Wesolowski

Argonne National Laboratory, Argonne, Illinois 60439

### SUMMARY

A prototype superconducting-helix accelerator is described and design considerations are discussed. The results obtained during 120 hours of beam acceleration are given. These include a wealth of practical engineering experience, the demonstration of stable operation with external phase control, and measurements of various kinds of accelerator-physics data.

### I. INTRODUCTION

A broad investigation of the technology of superconducting-accelerating structures is being carried out at Argonne in support of a proposal to construct a heavy-ion accelerator consisting of a 20-MV tandem injector and a superconducting-linac energy booster. Because of the low velocities of the heavy ions incident from the tandem, we have concentrated on the development of helical accelerating structures made of anodized niobium metal. There are three major components to the development program; (1) a study of the most critical questions concerning technical feasibility, (2) the construction and operation of several prototype accelerators, and (3) a search for economical solutions to the practical engineering problems.

The scope of the first phase of this program has been outlined recently<sup>1</sup>. The second (prototype) stage is progressing rapidly and is the focus of this paper. The third stage is just starting in earnest, although a great deal of valuable engineering experience is being acquired during the course of the prototype-accelerator work now in progress.

Our primary initial objective in the construction of prototype accelerators was to test in practice the solutions to the major technical problems being studied individually. In particular, the accelerator experiments afford excellent tests of what are thought to be the three major questions concerning the superconducting-helix accelerator: (1) stability of the RF properties of the accelerating structure, (2) control of mechanical vibrations, and (3) radiation damage of the anodized surface. As we have gotten into the prototype accelerator work, however, we have become increasingly aware that there are many other benefits. These include tests of possible difficulties such as contamination of the superconductor by the beam line, a clarification of vibration levels in an accelerator environment, information on beam dynamics for a non-ideal helix, and tests of acceleration calculations based on low-power field measurements. Perhaps even more important is being forced to face up to numerous engineering difficulties, and the fact that no entirely unexpected difficulties have developed.

Our prototype-accelerator program, as now conceived, has three phases: (1) acceleration tests with single  $\lambda/2$  structures, (2) acceleration tests with an expanded accelerator system consisting of a pair of  $\lambda/2$  structures that are independently controlled by a common master oscillator, and (3) the construction and beam testing of a resonator consisting of several tightly-coupled  $\lambda/2$  units within a common dewar. The first phase has just been completed, the second stage is now starting with the installation of the second accelerating structure, and the third stage is being planned.

### II. EXPERIMENTAL SYSTEM

The layout of the dual-helix prototype accelerator is shown in Fig. 1. The single-helix system for which results are reported here is identical except that the second unit is replaced by a piece of beam line. The velocities of the protons provided by the Van de Graaff injector are in the same range ( $\beta = 0.025 - 0.07$ ) as those of heavy ions from a 20-MV tandem. These proton beams are formed into short bursts by an RF chopper, bent by a magnet, accelerated by the helix, focused (if necessary) by a quadrupole pair, and finally detected and analyzed in both energy and time.

#### Beam Injection

An existing electron Van de Graaff (VDG) was converted to positive-ion operation to provide a dc beam of protons. The usable energy range is 0.3 to 2.5 MeV. Variations in terminal voltage, including ripple, are limited by voltage-controlled feedback to  $< 2$  kV peak-to-peak.

The dc beam is formed into discrete pulses by a chopper that operates synchronously with the superconducting-helix resonator. Space limitations along the beam-line and the need for beams with a wide range of low velocities ( $\beta = 0.025$  to  $0.07$ ) dictated the choice of a conventional RF-chopper system. With maximum deflection voltage, the incident dc beam can be chopped into pulses as short as 0.6 ns (FWHM), with a peak amplitude of 200  $\mu$ A and a repetition rate that is synchronous with the field of the helix.

A conventional magnet bends the beam through  $15^\circ$  and separates the several ion species. Thus far, only  $H^+$  has been accelerated.

#### Vacuum

Care was exercised in the design and installation of the beam-line in order to provide a relatively clean vacuum system. With the exception of the helices, the entire line was constructed of stainless steel. All seals are of metal.

Differential beam-line pumping is used both up- and downstream from the helices in order to provide partial isolation from the poor vacuum of the VDG and from possible leaks and outgassing in the region of the diagnostic instrumentation. The pumping arrangement (Fig. 1) provides stepwise isolation and results in a 100-fold improvement in the vacuum just downstream from the first helix ( $7 \times 10^{-8}$  T before helix cool down) in comparison with that at the VDG ( $7 \times 10^{-6}$  T).

Analysis of the residual gas (from 2 to 90 AMU) in the beam line was done prior to each helix cool down, periodically throughout the cool-down and warm-up cycles, and during acceleration tests. Aside from some hydrogen from the VDG, the observed spectra are typical of those expected for a clean unbaked-metal system.

#### Cryostats & Cryogenics

The cryostats (Fig. 2) have an outer vacuum jacket, an inner helium vessel, and an annular liquid-nitrogen radiation-shield tank in the insulating vacuum between

them; the vacuum jacket is an integral part of the beam line. Ports through the inner and outer vessels allow passage of the beam. The superfluid-helium bath is separated from the beam-line vacuum with indium seals between the beam ports of the niobium cavity and flanges mounted on short bellows welded into the helium vessel. The cover plate of the cryostat forms the helium-bath vacuum seal and provides a base from which the helix resonator is suspended by means of two RF-probe lines. Degaussing coils and a double shield of 0.8 mm thick  $\mu$  metal reduce the magnetic field at the helix to 5 mG during cool down.

The resonator is cooled by being immersed in the liquid-helium bath. The helix, made of niobium tubing, is open to the bath at both ends, and superfluid cooling occurs. The cryogenics system is designed to allow uninterrupted operation at temperatures below the lambda point.

The cryostat for each resonator is connected by a permanent nitrogen-cooled helium-transfer line to a 100-liter storage dewar. The cryostats are pumped to about 12 Torr by a mechanical booster pump so as to reduce the temperature of the helium bath to 1.8°K or below. Each cryostat<sup>2</sup> contains a heat exchanger and a Joule-Thompson expansion valve. Incoming liquid is cooled by outgoing boil-off gas before expanding through the J-T valve into the low-pressure region.

The consumption of liquid helium by the cryostat and its cryogenic system is about 3 liters/hr at an operating temperature of ~ 1.8°K. Specific details of the cryostat design and operating conditions are given in Ref. 3.

### Accelerating Structures

Two different  $\lambda/2$  cavities having rather different phase velocities were used in the acceleration tests. An assembled unit mounted in its cryostat is shown in Fig. 3. Parameters of each cavity are given in Fig. 4. Both units were fabricated of niobium metal, annealed at 1250°C, electropolished, and anodized by techniques that are similar to those reported previously<sup>1,4</sup>.

### RF Controls

Accelerator tests were conducted under two different modes of RF control. In the first mode, the helix served as the frequency-controlling element of a self-excited oscillator to which the chopper's RF system was synchronized. In the second mode, both the chopper and the helix were independently locked to an external master oscillator. Discussion of the latter system is given in Ref. 5. The first mode of operation was used to obtain accelerator-physics data on the helix structure and to acquire operating experience while the phase-lock circuitry was being readied.

### Mechanical Vibrations

The prototype accelerator was constructed in the existing housing for the VDG, and consequently it is in a conventional environment. Existing water and vacuum pumps, power transformers, ventilation fans, and the VDG-belt drive are necessary for the functioning of the facility. Also, the foundation mat and floor of the housing are internally tied to the cyclotron-linac complex (Bldg. 211), which includes a machine shop. In view of this overwhelming potential for external sources of vibration, the area was surveyed to obtain information on the intensity and sources of possible disturbances. The results range from a vibrational acceleration of ~ 0.01 g on the floor under the cryostats to 1 g on the VDG turbopump.

In order to minimize the coupling of external vibrations to the low-frequency modes<sup>1</sup> of the helix, conventional soft bellows were used along the beam line (Fig. 1). The RF-frequency variation in the resonator resulting from mechanical vibrations were found to be as low as  $\pm 125$  Hz. Considering the nature of the environment and the simplicity of the vibration isolation, these results are quite encouraging for future designs.

### Diagnostic Equipment

Beam alignment and focusing can be checked at various positions along the beam-line by viewing fluorescing quartz disks located at viewing ports, and by measuring the current hitting movable insulating slits (Fig. 1).

After the beam passes through the helix, both its energy and time structure can be measured by scattering protons from a thin gold foil onto a surface barrier silicon detector. This spectrometer was the principle diagnostic tool of our acceleration experiments. The intrinsic resolution width of the detector is 6 keV (FWHM), the measured resolution width of the proton beam was about 7.5 keV, and the overall timing jitter was less than 0.2 ns. An example of data obtained with this system is given in Fig. 5.

The energy of the beam can also be measured by means of the analyzing magnet shown in Fig. 1. This system was tedious to use but it has a much narrower resolution width than the pulse-height spectrometer.

Because of its speed and convenience, most of the measurements were made with the pulse-height spectrometer, with which a good spectrum could be measured in a few minutes of running time. The energy gain was usually measured with an accuracy of ~ 1%.

The pulse-height spectrometer was calibrated in three ways: (1) from the energy of the proton beam, as measured with the analyzing magnet, (2) from the pulse height for the 4.8236-MeV line from a <sup>233</sup>U alpha source, and (3) from the 922-keV resonance in the reaction Al<sup>27</sup>(p, $\gamma$ ). All three methods checked within a few keV.

## III. RESULTS OF ACCELERATION TESTS

The acceleration characteristics of two helices, units E and G, have been studied during some 120 hours of beam-acceleration time. The total time that these units have been cooled down on the beam line is some 1400 hours. The fact that a rapidly assembled system operated well and without a single breakdown for such a long time is one of our principle technological results.

Aside from the basic fact that the prototype accelerator functioned, the highlight of the work is that it proved possible to control electronically the vibration-induced RF-frequency variations and to phase-lock the helix resonator to a master oscillator at the relatively high field of 1.3 MV/m. The phase-lock system operated stably for long periods of time and was insensitive to perturbations by the incident proton beam. As discussed in Ref. 5, the present field limit of 1.3 MV/m appears to be set by purely practical difficulties, and it is realistic to expect that it will soon be feasible to phase-lock a functioning helix at the design field of > 2.0 MV/m.

The acceleration data provide several valuable checks on our understanding of the accelerating fields in helices. The absolute magnitudes of the measured energy gains are in excellent agreement with what had been inferred from theoretical calculations and from field measurements on low-power copper models. Also,

the dependence of the energy gain on the incident energy is in good agreement with what is expected, although we were initially surprised at how little dependence there is. Finally, our studies of accelerated beams show that the helix disturbs the direction of the incident projectile only slightly. All of these accelerator-physics results give one confidence that the dynamics of beams accelerated by helices can be calculated reliably from field measurements on low-power models.

Let us now consider the results in more detail.

### Energy-Gain Measurements

The energy gain provided by the helix was measured both with the pulse-height spectrometer, as illustrated in Fig. 5, and with the magnetic analyzer, as illustrated in Fig. 6. In the latter, one sees that the energy spread of the accelerated beam is not measurably greater than that of the incident beam. Incidentally, the data in Fig. 6 were obtained while the phase of the helix was being controlled by the external master oscillator.

### Phase-Angle Dependence

When the energy gain  $\Delta T$  of the projectile is not too great, one expects  $\Delta T$  to vary as  $\cos \phi$ , where  $\phi$  is the phase at which the beam pulse passes through the center of the helix. Thus, the phase-angle dependence provides a good test of the proper functioning of the entire system. A typical result is given in Fig. 8, where the quality of the data and the fit are seen to be excellent. Since we can easily determine only the quantity  $[\phi(\text{helix}) - \phi(\text{chopper}) + \text{const.}]$ , in Fig. 8 the zero in  $\phi$  has been adjusted to fit the data.

### Dependence on Incident Energy

The dependence of the energy gain  $\Delta T$  on the incident energy  $T_i$  was carefully measured for both Helix E and Helix G. The results obtained for  $\phi = 0$  are given in Fig. 7, where the abscissa is  $(T_i + 1/2 \Delta T)$ . Since the accumulation of each set of data extended over a period of some 30 hours, the smooth variation of the data points suggests a high degree of stability of the system. In fact, the measurements seemed to be completely reproducible over a period of days.

For Helix E, the dependence of  $\Delta T$  on  $T_i$  can be explained well in terms of what is calculated from field measurements on a low-power model. Assume that the axial field  $E_z$  may be described by

$$E_z = \sin(2\pi ft + \phi) \sum_n E_n \sin \frac{2\pi z}{\lambda_n}, \quad (1)$$

where the  $E_n$  and  $\lambda_n$  are constants. Then the energy gain can readily be shown to be (for  $\Delta T/T \ll 1$ )

$$\Delta T = \frac{1}{2} q L \cos \phi \sum_n E_n t_n, \quad (2a)$$

where

$$t_n = \frac{\sin \pi \left(1 - \frac{v_n}{v}\right) \frac{L}{\lambda_n}}{\pi \left(1 - \frac{v_n}{v}\right) \frac{L}{\lambda_n}} - \frac{\sin \pi \left(1 + \frac{v_n}{v}\right) \frac{L}{\lambda_n}}{\pi \left(1 + \frac{v_n}{v}\right) \frac{L}{\lambda_n}}. \quad (2b)$$

Here  $t_n$  is the transit-time factor for the  $n^{\text{th}}$  component,  $v_n = f\lambda_n$  is the synchronous velocity corresponding to  $\lambda_n$ , and  $L$  is the length of the field region described by Eq. (1). The first term of Eq. (2b) results from the forward-travelling wave and the second term from the backward wave.

Beam measurements on the low-field model of Helix E specify  $E_z^2$  vs  $z$ . The curve of  $E_z$  vs  $z$  deduced from these data is somewhat asymmetrical, but it can reasonably be approximated by a single sine function. The effective wavelength (18.3 cm) associated with this single-term description of  $E_z$  was used to calculate the transit-time factor from Eq. (2). The result ( $\Delta T/\Delta T_S \equiv t$ ) is the solid curve in Fig. 7; here  $\Delta T_S$  is the energy gain for the synchronous particle. The fit is excellent, again emphasizing the stability of the acceleration system.

The dash line associated with the data of Helix G is similar in meaning to the other curve. However, for G we do not yet have refined field measurements, and hence the curve was calculated by adjusting the helix-wavelength parameter to obtain a fit.

An interesting aspect of the data of Fig. 7 is that the transit-time factor is greater than unity for some energies; that is, the particle with the synchronous velocity does not experience the maximum energy gain in a short helix. This initially surprising result comes about because the backward wave contributes a significant energy gain to particles traveling somewhat faster than the synchronous velocity. From a practical point of view, the observed energy dependence means that a  $\lambda/2$  helix of a given design is suitable for a wide range of incident energies.

### Absolute Value of the Accelerating Field

Heretofore, our estimates of accelerating fields in superconducting helices have been based on field-probe measurements in low-power copper models. The acceleration data provide a direct check on the reliability of the procedure. The accelerating-field values  $E_{ax}$  given in this paper are defined by

$$E_{ax} = \Delta T_S / (\text{Helix Length}), \quad (3)$$

where  $\Delta T_S$  is the energy gain at  $\phi = 0$  for particles with the synchronous velocity. This quantity is the same as the usual definition of the accelerating field (traveling wave) for a long helix for which the PQ product per  $\lambda/2$  section is the same; i.e., we intend that  $E_{ax} \approx E_{ax}^{\text{long}}(\text{long helix})$ . The equivalence may be checked by comparing the calculated energy gain for a long helix with the gain for an equivalent short helix. The long-helix gain calculated from the sheath model and the short-helix gain deduced from our field measurements on a model of Helix E are the same within  $\sim 6\%$ .

Experimentally, it is most convenient to determine  $E_{ax}$  from the static frequency shift  $\Delta f$  caused by radiation pressure. Arguments based on general considerations indicate that  $E_{ax} = k \sqrt{\Delta f}$ . Values of the constant  $k$  determined from the observed shift  $\Delta f$  and the acceleration data are 0.078 and 0.138 for Helices E and G, respectively. The constant  $k$  may also be determined by combining the data from field, power-loss  $P$ , and  $Q$  measurements on a room-temperature helix with those from  $P$ ,  $Q$ , and  $\Delta f$  measurements at 1.8°K. The result obtained for Helix G is  $k = 0.136$ . The excellent agreement between the values of  $k$  obtained in entirely different ways is gratifying.

### IV. PLANS FOR THE FUTURE

Our development program will continue to be directed both toward understanding the phenomena involved in superconducting accelerating structures and toward the engineering of such systems. Within the next few weeks, acceleration with the two-helix assembly will be initiated and directed towards achieving the design

goal of complete external control of the RF acceleration fields. We will continue to study surface effects, materials, radiation-damage effects of heavy ions, the statistics of reproducibility of anodized cavities, and the optimization of design parameters.

Within the next few months, new programs will be initiated, including the design of a new prototype accelerator involving two resonators, one of which has 5 closely-coupled  $\lambda/2$  sections in a common dewar. This program is intended to demonstrate the feasibility of a different kind of module and to provide answers to important questions relating to engineering design.

References

\*Work performed under the auspices of the U.S. Atomic Energy Commission.

- (1) R. Benaroya, A. H. Jaffey, K. Johnson, T. Khoe, J. J. Livingood, J. M. Nixon, G. W. Parker, W. J. Ramler, J. Aron, K. E. Gray, and W. A. Wesolowski, Proc. 1972 Proton Linear Accelerator Conference (Los Alamos, October 10, 1972), p.168
- (2) Designed and built to ANL specifications by Gardner Cryogenics Div. of Carpenter Technology Corp.
- (3) J. Nixon, Cryostats 1F1 Superconducting Prototype Accelerator, Internal Bldg. 211 (ANL) Design Note, JMN 60 (1973)
- (4) R. Benaroya, A. H. Jaffey, K. Johnson, T. Khoe, J. J. Livingood, J. M. Nixon, G. W. Parker, W. J. Ramler, J. Aron, and W. A. Wesolowski, Appl. Phys. Lett. 21, 235 (1972)
- (5) O. D. Despe, K. W. Johnson, and T. K. Khoe, "Vibration-RF Control of Superconducting Resonators for Heavy-Ion Acceleration", Paper B-7, this Conference.

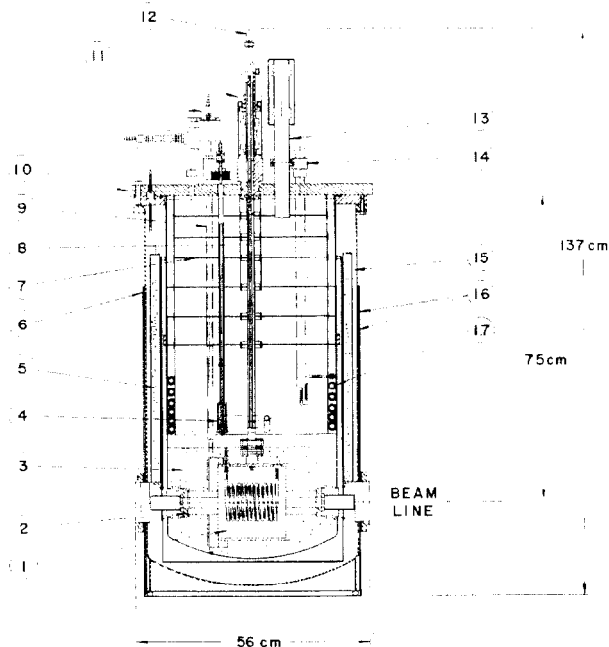


Fig. 2 Cross-section of the beam-line cryostat: (1) Resonator, (2) Indium Seals, (3) LHe Bath, (4) J-T Valve, (5) LN<sub>2</sub>, (6) Degaussing Coils, (7) Cu Heat Shields, (8) RF Probes, (9) Level Sensor, (10) Support Plate, (11) Adjustment Mechanism for RF Probes, (12) RF Input, (13) Vacuum Pump-out, (14) LHe Input, (15) Vacuum Shield, (16) Mu Metal Shields, (17) Heat Exchanger.

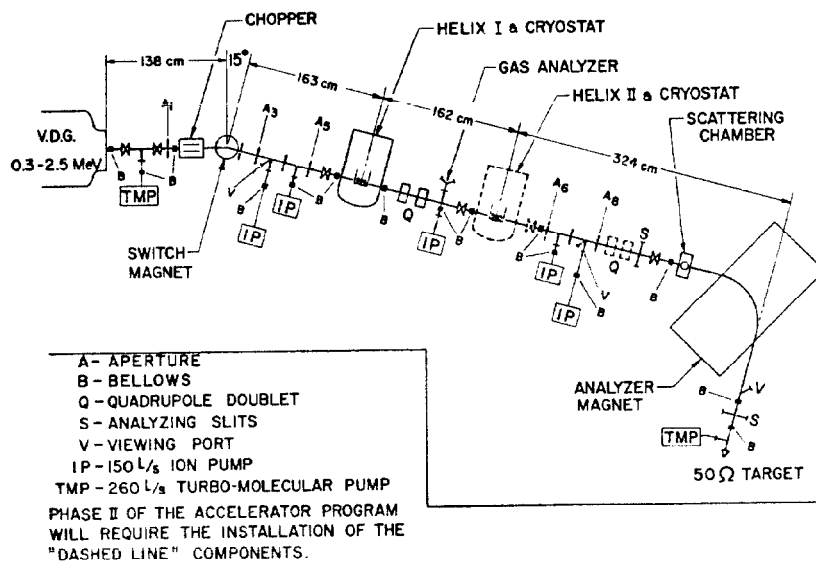


Fig. 1 Arrangement of the Prototype Superconducting Accelerator

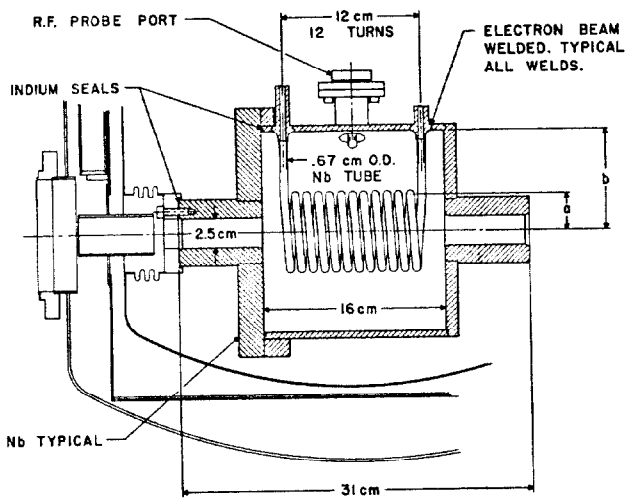


Fig. 3 Cross-section of the helix resonator

Unit	Helix Radius a	Cavity Radius b	Pitch	Tubing Diameter	Helix Length
E	4.40	8.80	1.016	0.66	12.19
G	3.30	8.80	1.016	0.66	12.19

Unit	Cavity Length	Number of Turns	$\frac{b}{a}$	Resonance Frequency (MHz)	$\beta$
E	16.00	12	2.0	63.1	0.038
G	16.00	12	2.66	91.6	0.053

(All dimensions in centimeters)

Fig. 4 Properties of the accelerating resonators. All dimensions are in cm.

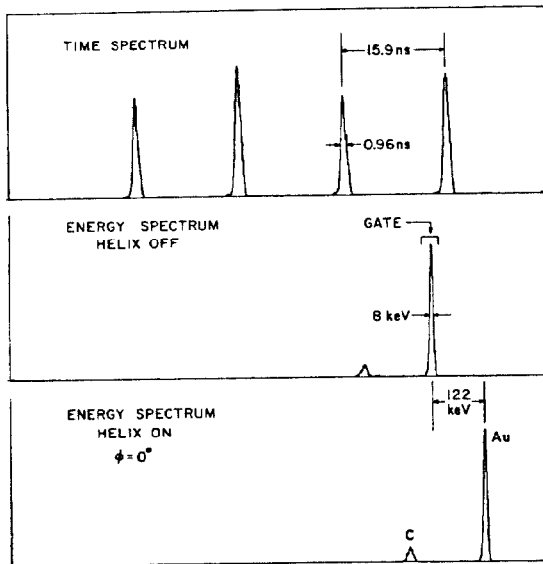


Fig. 5 Typical time- and energy- spectrum with silicon diode

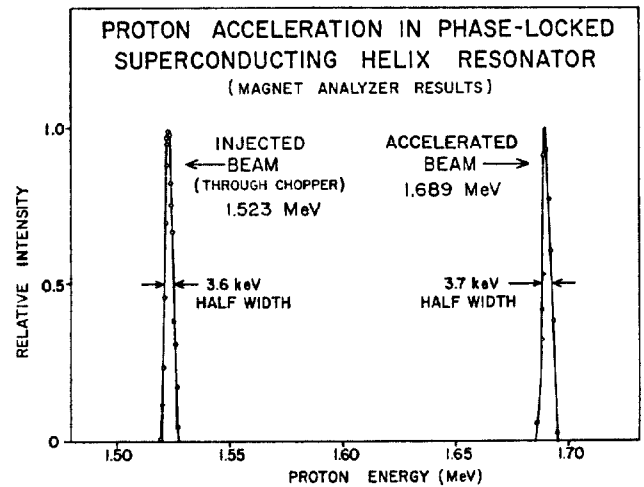


Fig. 6 Acceleration by phase-locked helix "G"

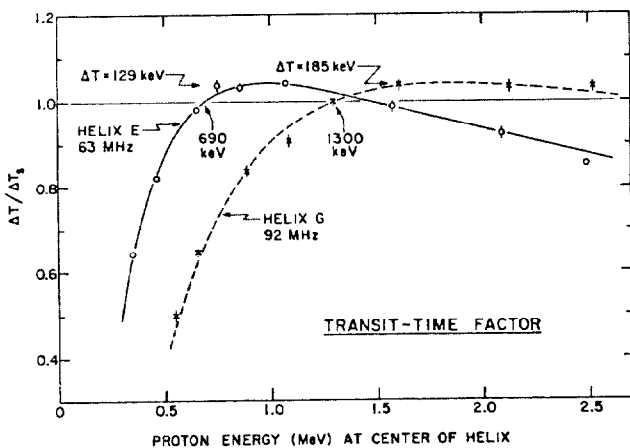


Fig. 7 Transit-Time Factors for two different helix structures ( $\beta_E = 0.038$  &  $\beta_G = 0.053$ )

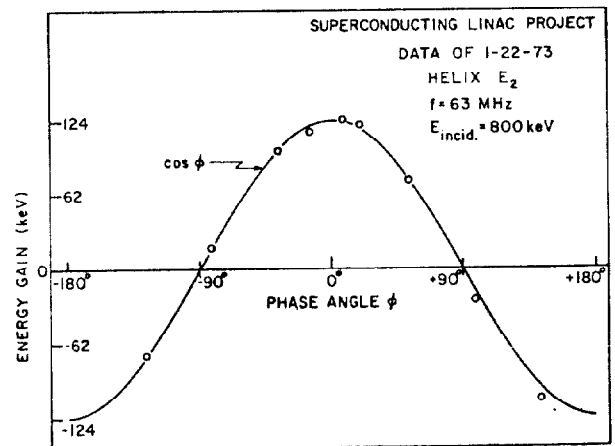


Fig. 8 Typical data showing dependence of energy gain on injection phase angle